11

Digital Demodulation of Interferometric Signals

Tristan J. Tayag and R. Collins Watson
Texas Christian University
USA

1. Introduction

The marriage of optical sensing techniques with sophisticated digital signal processing has resulted in a myriad of practical metrology systems. Optical metrology systems offer many attractive measurement features. These systems are inherently non-contacting, non-destructive, and immune from electromagnetic interference. In addition, since light is used as the sensing probe, the measurement system is capable of high sensitivity, fine resolution (both spatial and temporal), and absolute calibration.

The leap from the vibration stabilized table of the laboratory to the harsh milieu of the factory floor has been a major challenge for optical metrology systems. However, on-going advances in digital processor speed and algorithmic complexity have in large part made this leap possible. Full-field optical inspection methods include holographic interferometry, speckle metrology, and interferometric computed tomography (Tayag & Bachim, 2010). These techniques have been applied to a wide range of applications in biological tissue characterization, the automotive industry, dentistry, the semiconductor industry (Pitt et al., 2003; Tayag et al., 2003; Tayag et al., 2010; Weber et al., 2004), and fiber optic and bulk optic characterization (Osten et al., 2010). Here, we focus our attention on digital demodulation applied to "point measurements" as opposed to full-field measurements.

In this chapter of *Modern Metrology Concerns*, we present recent digital signal processing techniques used in interferometry. Application areas range from biotechnology to industrial to military. Specific examples will be cited throughout the literature as well as from our own research. Our research in digital demodulation techniques include applications in myofibroblast cell contraction (Kern et al., 2003), ballistic shock characterization (Kumar et al., 2009), and down-hole oil well drilling. In addition, we present a new (unpublished) digital demodulation algorithm. The novelty of our technique lies in the frequency domain manipulation of the well-known phase-generated carrier modulation approach.

Section 2 contains background information on interferometry and practical modulation techniques. The Michelson, Mach-Zehnder, Sagnac, and Fizeau optical configurations will be described. Once the basic optical geometries are established, we describe the modulation and demodulation techniques which are needed in practice. These techniques convert the measured phase change into the desired displacement, velocity, or index change.

Our novel digital demodulation algorithm will be presented in Section 3. The application of this research is in sensing down-hole drill bit parameters for oil well drilling systems. We present a new demodulation algorithm for phase-generated carrier based interferometers. The theoretical background is presented along with simulation results.

Section 4 will follow with a summary and directions for future research.

2. Interferometry

Measurements made with interferometers are based on the interference pattern formed by two or more electromagnetic fields. In this discussion, we confine ourselves to the interference of two electromagnetic fields in the visible region of the spectrum. A stable fringe pattern results when the two interfering fields satisfy the following conditions:

- The two fields have the same optical wavelength.
- The two fields maintain a fixed phase relationship.
- Each of the two fields has its electric field vector linearly polarized.
- The two fields have collinear polarization vectors.

To achieve these conditions, the source may be a linearly polarized single mode (temporal and spatial) laser. The light from this laser is split into two beams known as the reference and signal beams. The output optical power resulting from the interference of these two fields takes the form of a raised cosine which varies as a function of the optical path length difference between the reference and signal beams (see Fig. 1).

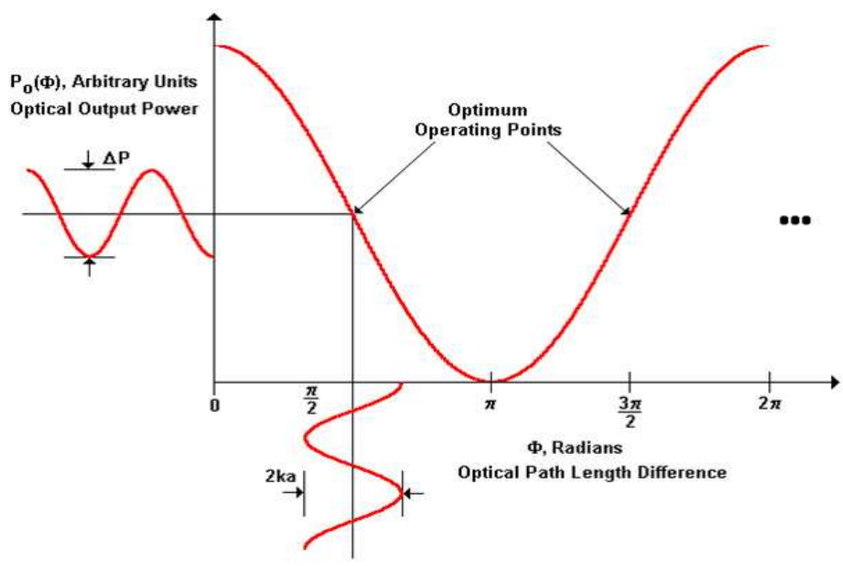

Fig. 1. Optical output power versus path length difference for an interferometer.

Practical metrology systems require fine resolving capabilities as well as large dynamic range. Fractional fringe interferometers are capable of resolving displacements that are many orders of magnitude less than the optical probe's wavelength. This high resolution is achieved when the interferometer is operated at quadrature, the point of maximum sensitivity. As shown in Fig. 1, operating the interferometer at quadrature yields large changes in the optical output power for small changes in the path length difference between the reference and signal beams. To achieve large dynamic range, interferometers may employ fringe counting techniques for changes in the optical path difference, which exceed half of the field's wavelength.

A number of two beam interferometric configurations have been developed over the past two centuries. In the next section, we will review four of these optical configurations.

2.1 Optical configurations

In 1881, the American physicist, Albert A. Michelson, developed the basic interferometric configuration shown in Fig. 2. Light from the optical source is split into the signal and reference beams with a beamsplitter. The reference beam reflects off a mirror and retraces its path. The signal beam reflects off the specular surface of the object whose displacement is to be measured. The two beams are recombined using the original beamsplitter. A portion of each of the reference and signal fields is incident on the detector. If the optical path length difference between the reference and signal fields is zero (or an integral multiple of wavelengths), the interference is constructive. If the optical path length difference is π (or an odd multiple of half wavelengths), the interference is destructive.

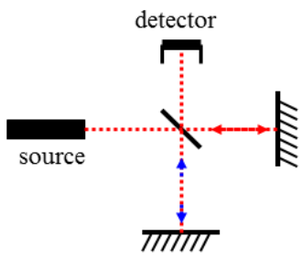

Fig. 2. Michelson optical configuration.

The Mach-Zehnder optical configuration shown in Fig. 3 provides flexibility over the Michelson configuration by using a second beamsplitter to combine the reference and signal beams. With the environment of the reference beam remaining constant, changes in the refractive index through which the signal arm passes may be measured. Because of its suitability for a "push-pull" arrangement, this configuration is used in optical modulator technology (Kaplan & Ruschin, 2000) as well as optical sensor technology (Porte et al., 1999).

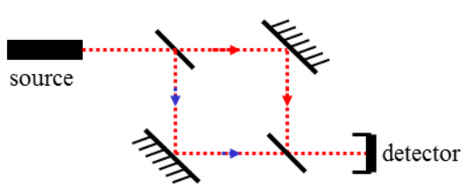

Fig. 3. Mach-Zehnder optical configuration.

The Sagnac or cyclic optical configuration is shown in Fig 4. This configuration is unique in that the two beams follow the same path around a closed circuit, but in opposite directions. This sensor measures the non-reciprocal phase changes that arise between light propagating in clockwise and counter-clockwise directions. In gyroscope sensing applications, the phase shift gives a measure of the rotation of the loop about its axis (Saida & Hotate, 1999; Barbour & Schmidt, 2001; Tselikov et al., 1998).

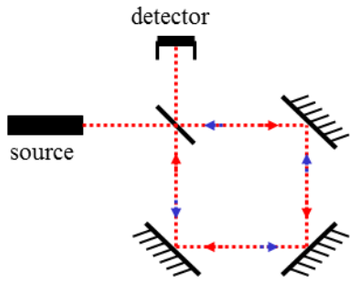

Fig. 4. Sagnac optical configuration.

The optical configuration shown in Fig. 5 is attributed to the French physicist, Hippolyte L. Fizeau. In this configuration, interference occurs between light reflected from the target and the partial reflection from the facet of the fiber probe. High stability (i.e., low phase drift) is a key advantage of this configuration since the fiber/target separation distance is typically very small to accommodate sufficient light coupling back into the fiber. Another advantage of this system is the common path travelled by the majority of the reference and signal beams. In the fiber optic embodiment shown in Fig. 5, this means that the single mode optical fiber does not have to be polarization preserving, since both beams will undergo the same polarization evolution as they travel through the fiber. Each of the interferometric configurations described in this section, encodes a displacement, index change, or rotation rate into a phase shift between two interfering light beams. Practical techniques for extracting the desired parameter from the phase shift information form the topics of the next section.

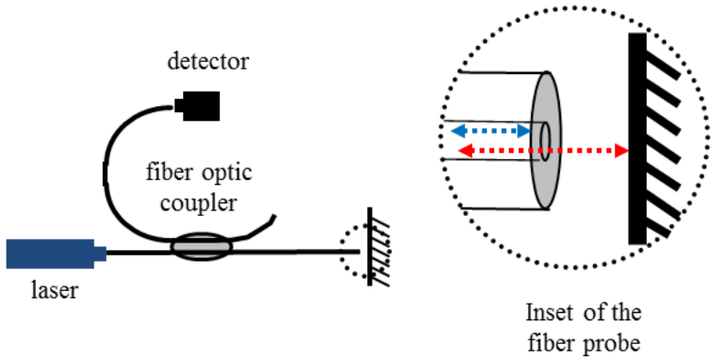

Fig. 5. Fizeau optical configuration.

2.2 Modulation and demodulation techniques

Interferometer modulation and demodulation techniques have been broadly classified into homodyne and heterodyne approaches. Homodyne modulation techniques refer to those systems where the two interfering beams of light are of the same optical frequency. The homodyne techniques may be further sub-divided into active homodyne and passive homodyne. In the early days of interferometry, the scientist would wait until the interferometer drifted into the quadrature operating point before starting data collection. Today, active feedback control is used to adjust the reference path and maintain the interferometer at quadrature. Digital signal processing of the modulated signal is applied to compute the feedback control signal.

In passive homodyne modulation, techniques are used to generate output signals which after digital processing eliminate the signal fading that occurs as the interferometer drifts from the quadrature condition. In this way, no feedback control loop is needed to maintain the optimum operating point.

Heterodyne modulation techniques refer to those systems where the two interfering beams have differing optical frequencies. A frequency shift in one of the beams may be accomplished by acousto-optic frequency modulation (Culshaw & Giles, 1982), frequency ramping the optical source (Jackson et al., 1982), or piezoelectric-induced path length changes (Jackson et al., 1980; Cole et al., 1982). These heterodyne modulation approaches have been categorized as true-heterodyne, pseudo-heterodyne, and synthetic-heterodyne techniques.

In practical application, the boundaries between the homodyne and heterodyne approaches as well as their sub-divisions become blurred. In the remainder of this section, we describe 3 digital demodulation methods for interferometric sensors.

The phase-generated carrier demodulation technique was first proposed by Dandridge, Tveten, and Giallorenzi in 1982 (Dandridge et al., 1982). It is a homodyne demodulation technique which eliminates signal fading as slow environmental perturbations drift the interferometer's path length difference away from quadrature. In this technique, a sinusoidal modulation with known frequency and amplitude is imposed on the interferometer's phase difference. Detection and mathematical manipulation of interferometer signal allow the desired phase shift to be separated from environmental perturbations. The signal processing involves detection of the signal amplitudes at the carrier's fundamental and second harmonic frequencies. The time derivative of each of these signals is computed and they are cross-multiplied with the original signals. Integration of the difference of these signals results in the desired phase change. We have analyzed the quantum-noise-limited sensitivity of interferometers using a phase-generated carrier modulation scheme (Tayag, 2002).

Dandridge et al. first demonstrated this phase-generated carrier demodulation technique using analog electronics. Since that time, a commercially-available demodulation system based on the phase-generated carrier has come on the market (Bush et al., 1996; Cekorich et al., 1997; Davis et al., 1998). This system is based on real-time digital processing of the interferometer's signal in the time domain. We have used this demodulation system to characterize the contraction of myofibroblast cells within a collagen matrix (Kern et al., 2003). In Section 3 of this chapter, we present a new demodulation algorithm whose kernel is based on a frequency domain analysis of the interferometer's phase-generated carrier signal.

The J1…J4 demodulation method (Sudarshanam & Srivivasan, 1989) is a passive homodyne technique which requires no feedback for stabilization of the interferometer at quadrature. This technique is applicable to measuring the amplitude of sinusoidally vibrating structures. In this approach, the photodetected interferometer output is expanded using a Fourier-Bessel series. In fact, the "J1…J4" name of this method refers to the $J_n(x)$ Bessel functions of the first kind of order n in the Fourier-Bessel expansion. Jin et al. (Jin et al., 1991; Jin et al., 1992) modified this method to extend the desired phase modulation index. Marcal et al. (Marcal et al., 2007) have used this digital demodulation technique with a Michelson interferometric configuration to characterize the frequency response of a novel piezoelectric actuator. We have used a similar digital demodulation algorithm to characterize

microelectromechanical system (MEMS) structures (Pitt et al., 2003). Our fiber optical configuration for this system was based on the Fizeau interferometer.

A final digital demodulation technique we will review is based on the use of a 3x3 fiber optic coupler in the optical system (Kwon et al., 1999; Sheem, 1981; Sheem et al., 1982). Again, the demodulation method is classified as a passive homodyne technique. The optical configuration is shown in Fig. 6 and is basically a Mach-Zehnder optical configuration, but uses a 3x3 fiber coupler to combine the beams. Koo, Tveten, and Dandridge (Koo et al., 1982) were the first to introduce this passive stabilization technique for fiber optic interferometers. Todd et al. (Todd et al., 1999) later applied digital demodulation techniques to Koo's 3x3 fiber coupler-based system.

The unbalanced path lengths and 3x3 coupler of the Mach-Zehnder interferometer shown in Fig. 6 are necessary for the interferometer to function as a wavelength discriminating sensor. The outputs from the 3 photodetectors are shifted from each other by $2\pi/3$ radians. With *a priori* knowledge of the coupler and detector characteristics, the post-detection digital processing can extract the interferometer's phase shift corresponding to a wavelength shift in the optical signal. This interferometric wavelength discriminator has been used to interrogate and multiplex a network of fiber Bragg grating sensors (Johnson et al., 2000) and as a velocity sensor which measures the Doppler shift in the light reflected from a moving surface (Fabiny & Kersey, 1997). We have also used this system as a Doppler velocimeter to measure the motion of armored plates experiencing ballistic shock (Kumar et al., 2009).

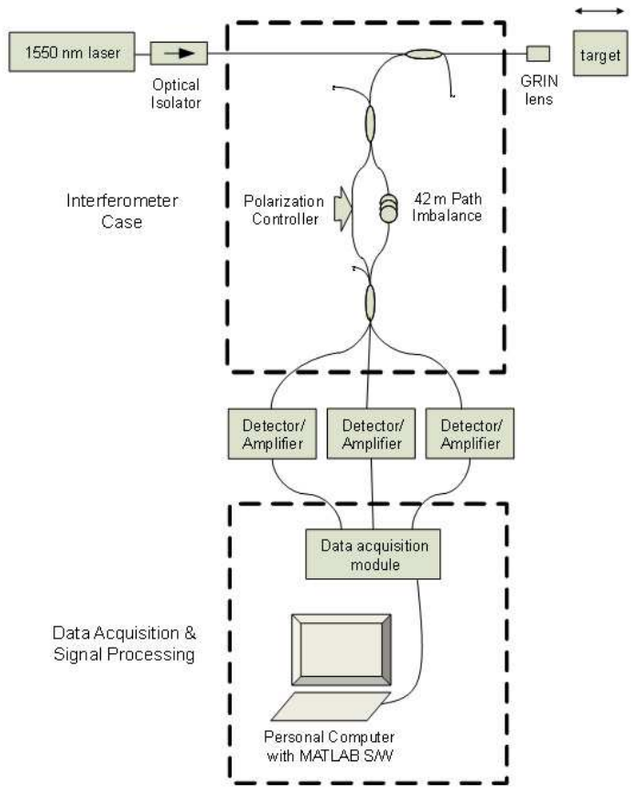

Fig. 6. Interferometric velocimeter based on a 3x3 fiber coupler and homodyne demodulation technique (Kumar et al., 2009).

2.3 Summary

In this section, we have reviewed the classical optical configurations and modulation/demodulation techniques of interferometric systems. There exists a close relationship between the optical configuration and the modulation technique. Our focus has been on those systems which exploit digital processing in their demodulation methods. It is interesting to note that all the interferometric systems we have presented are based on passive homodyne demodulation. This is not surprising, since the digital processor and its associated demodulation algorithm are replacing the optical hardware (acousto-optic modulators or swept frequency lasers and their drive electronics) and electronic hardware (piezoelectric transducers, analog differentiators, integrators, and lock-in amplifiers) necessary in active homodyne and heterodyne systems. In this way, the overall interferometric system is greatly simplified with the burden of complexity falling on the software. This results in a more robust and less expensive metrology system.

3. Frequency domain demodulation of a phase-generated carrier

Since the time and frequency domains represent different ways of describing the same signal, it is reasonable to consider an algorithm based on frequency domain analysis as an alternative to the phase-generated carrier time domain algorithm discussed in the previous section. In this section, we describe the kernel of a novel algorithm for the demodulation of an interferometric signal based on a phase-generated carrier modulation scheme. Following this section, practical implementation of the algorithm is discussed with simulation results verifying the algorithm. Finally, the frequency domain demodulation algorithm is summarized with suggestions for further research.

3.1 Algorithmic development

Two-beam interferometers produce an optical interference pattern, which varies with optical path length difference, $R(t)$, between a signal arm and a reference arm. It is well-known that the optical power, $P(t)$, of this interference pattern, takes the form

$$P(t) = P_{dc} + P_{ac}\cos\left[R(t)\right],$$

where P_{dc} is the dc optical power and P_{ac} is the *0*-to-peak modulation index of the interference pattern. This optical power is incident on a photodetector for conversion to an electronic signal. Since *PIN* photodiodes are characterized by a responsivity, which is constant with respect to the incident optical power, the photo-generated current takes the same mathematical form of a raised cosine. If the electronic signal from the receiver is a voltage, then this signal takes the form

$$V(t) = V_{dc} + V_{ac}\cos\left[R(t)\right],$$

where V_{dc} is the dc voltage level and V_{ac} is the *0*-to-peak modulation index of the interference pattern. The objective of the demodulator is to sample this electronic signal, process the signal samples in real-time to determine the phase $R(t)$, and produce an analog signal output, which is proportional to the phase $R(t)$.

The demodulation algorithm is based on a phase generated carrier modulation technique. A key assumption is that a sinusoidal carrier signal is imposed on the interferometer's optical signal such that the interference pattern becomes

$$V(t) = V_{dc} + V_{ac}\cos\left[R(t) + M\sin\left(2\pi Ft + W\right)\right], \tag{1}$$

where M is the phase index of the sinusoidal carrier, F is the frequency of the carrier, and W is the phase of the carrier. Since the sinusoidal carrier appears as a phase term in the interferometer's cosinusoidal interference pattern, this form of modulation is referred to as a "phase-generated carrier."

The output voltage of Eqn. (1) describes the interferometer's output signal. Let us rewrite this equation with the angular frequency of the carrier signal defined by $\omega_o \equiv 2\pi F$ rad/s:

$$V(t) = V_{dc} + V_{ac}\cos\left[R + M\sin\left(\omega_o t + W\right)\right]. \tag{2}$$

We may set our sinusoidal carrier signal such that $M = \pi$ rad and $W = 0$ rad. Then Eqn. (2) becomes

$$V(t) = V_{dc} + V_{ac}\cos\left[R + \pi\sin\left(\omega_o t\right)\right]. \tag{3}$$

Trigonometric expansion of the cosine term yields

$$V(t) = V_{dc} + V_{ac}\left\{\cos[R]\cdot\cos\left[\pi\sin\left(\omega_o t\right)\right] - \sin[R]\cdot\sin\left[\pi\sin\left(\omega_o t\right)\right]\right\}. \tag{4}$$

Now, note the Bessel expansions

$$\cos\left[\pi\sin\left(\omega_o t\right)\right] = J_0(\pi) + 2\sum_{n=1}^{\infty} J_{2n}(\pi)\cos\left[\left(2n\right)\cdot\omega_o t\right] \text{ and} \tag{5}$$

$$\sin\left[\pi\sin\left(\omega_o t\right)\right] = 2\sum_{m=1}^{\infty} J_{2m-1}(\pi)\sin\left[\left(2m-1\right)\cdot\omega_o t\right], \tag{6}$$

where $J_n(x)$ is a Bessel function of the first kind of order n. Substitution of Eqns. (5) and (6) into Eqn. (4) reveals the harmonic content of the interferometric signal in the frequency domain as

$$\begin{aligned} V(t) = &\left[V_{dc} + V_{ac}\cos\left(R\right)J_0\left(\pi\right)\right] \\ &- 2V_{ac}\sin\left(R\right)J_1\left(\pi\right)\sin\left(\omega_o t\right) \\ &+ 2V_{ac}\cos\left(R\right)J_2\left(\pi\right)\cos\left(2\omega_o t\right) \\ &- 2V_{ac}\sin\left(R\right)\sum_{m=2}^{\infty} J_{2m-1}\left(\pi\right)\sin\left[\left(2m-1\right)\cdot\omega_o t\right] \\ &+ 2V_{ac}\cos\left(R\right)\sum_{n=2}^{\infty} J_{2n}\left(\pi\right)\cos\left[\left(2n\right)\cdot\omega_o t\right]. \end{aligned} \tag{7}$$

The first and second harmonics of $V(t)$ are

$$V_{\omega_o}(t) = -2V_{ac}\sin(R)J_1(\pi)\sin(\omega_o t) \text{ and} \tag{8}$$

$$V_{2\omega_o}(t) = 2V_{ac}\cos(R)J_2(\pi)\cos(2\omega_o t)\,. \tag{9}$$

These two frequency components contain sufficient information to determine the desired phase, R. By taking the ratio of the amplitudes of these frequencies, the dependence on the interference pattern's modulation index V_{ac} is removed. The Bessel functions are known constants, which may be removed from the ratio as follows:

$$-\frac{J_2(\pi)\left[V_{\omega_o}(t)\ \text{amplitude}\right]}{\mathrm{J}_1(\pi)\left[V_{2\omega_o}(t)\ \text{amplitude}\right]} = \frac{\sin(R)}{\cos(R)} = \tan(R)\,. \tag{10}$$

The phase R may be computed from this quotient over an entire 2π rad phase range using an inverse tangent approximation. This forms the kernel of the frequency domain demodulation algorithm. A fringe counting approach similar to that described by Cekorich (Cekorich, 1999), may be used to extend the range of demodulation. In the next section, we describe practical DSP techniques to implement the frequency domain demodulation algorithm.

3.2 Simulation results

We have verified the frequency domain demodulation algorithm through computer simulation. In this section, we present those simulation results and describe our DSP implementation approach. The frequency spectrum of the interferometer's output signal is shown in Fig. 7. The magnitude spectra are shown for the five different values of the desired phase R. The periodic nature of the time domain signals correctly results in a set of discrete, harmonically-related sinusoids in the frequency domain. The open circles in Fig. 7 indicate the fundamental and second harmonic frequencies which are oscillating at ω_o and $2\omega_o$, respectively. Note the consistency between the magnitude spectra of Fig. 8 and Eqns. (8) and (9). Specifically, the zeros are apparent at ω_o for $R = 0$ and π rad and at $2\omega_o$ for $R = \pi/2$ rad. As described by Eqn. (10), these two frequency components will be used to demodulate the interferometer.

A significant aspect of the frequency domain algorithm is the conversion of the sampled time domain signal into a frequency domain representation. Computation of the frequency spectrum is conveniently performed via the well-known fast Fourier transform (FFT) algorithm. Since only 2 spectral components are required for this algorithm, the Goertzel algorithm provides a slightly more computationally efficient approach. We implemented both algorithms, but only present the results for the FFT algorithm here since the Goertzel results are equivalent.

The FFT algorithm results in complex-valued signals at each frequency bin. The magnitudes of these complex signals are shown in Fig. 7. Fig. 8 illustrates how the magnitudes of the

fundamental and second harmonics vary with the phase, R. These plots are consistent with the mathematical form given in Eqns. (8) and (9). The difference in peak amplitudes results from the Bessel function weighting factors, i.e. $J_1(\pi) = -0.5692$ and $J_2(\pi = 0.9709)$. Note that the magnitude spectrum contains only positive values. Therefore, the magnitude spectrum alone is insufficient to unambiguously determine R. To resolve R over the full 2π phase interval, the phase spectrum is also needed. Fig. 9 shows the phases of the fundamental and second harmonics as a function of R.

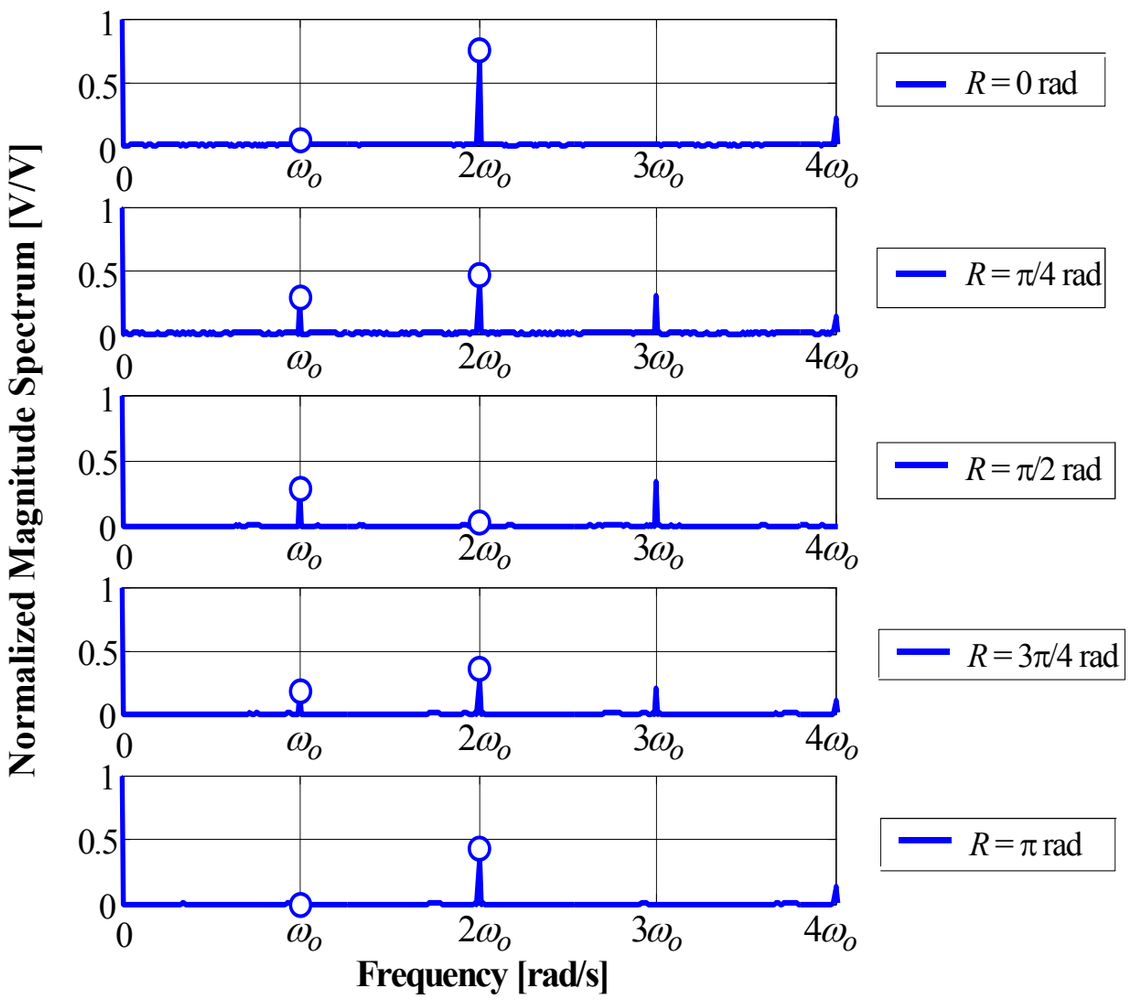

Fig. 7. Normalized frequency spectra of the interferometer signal described by Eqn. (7) at five different values of the phase R. The open circles represent the values of the fundamental and second harmonic frequency components.

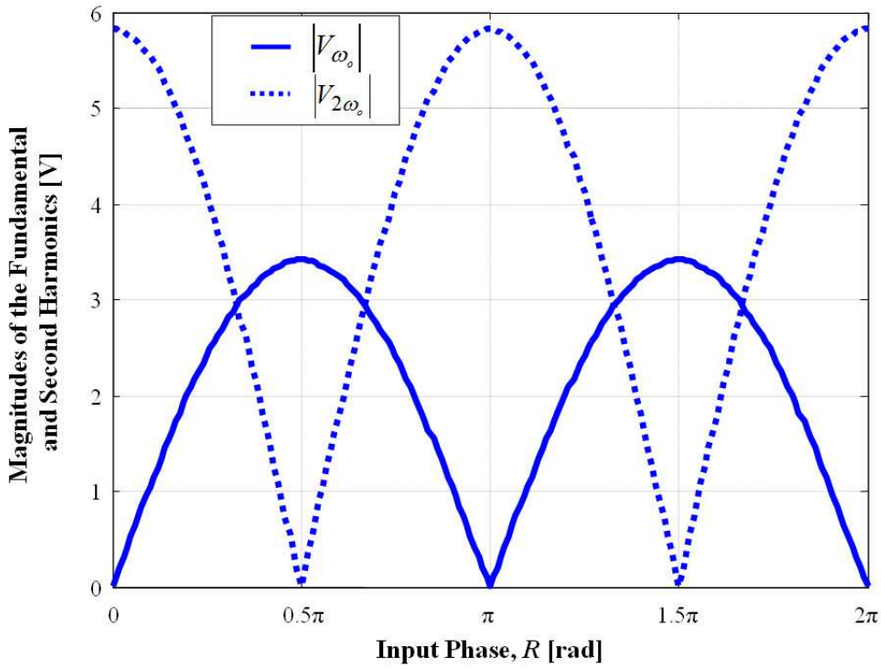

Fig. 8. Magnitudes of the fundamental and second harmonic frequencies as a function of the phase R.

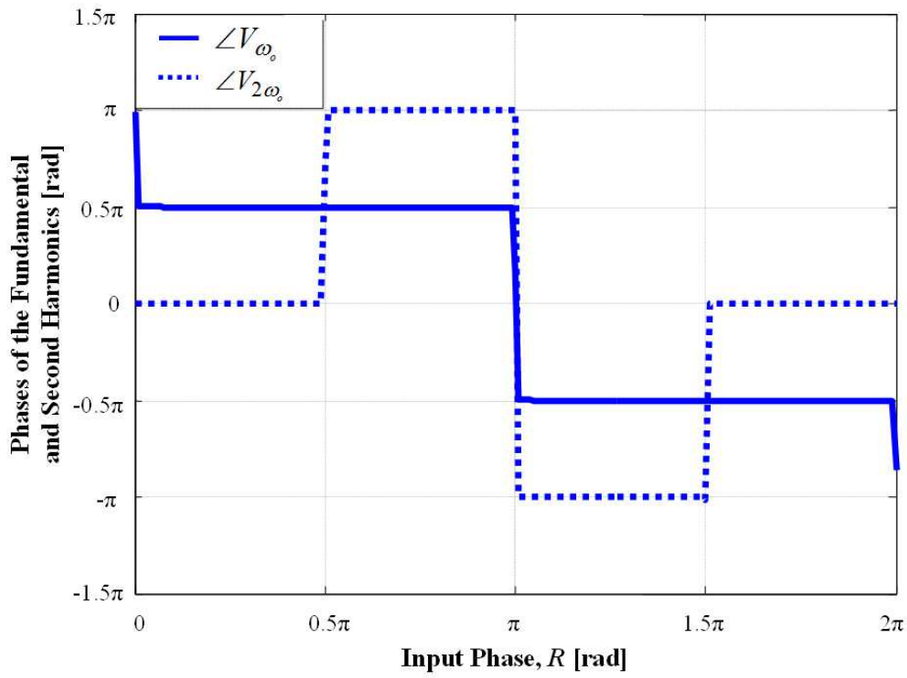

Fig. 9. Phases of the fundamental and second harmonic frequencies as a function of the phase R.

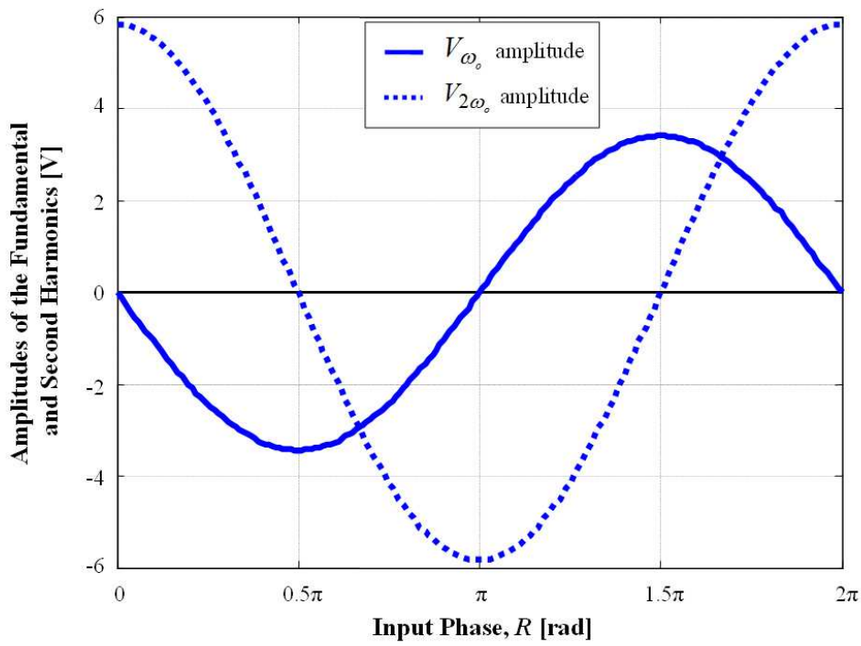

Fig. 10. Reconstructed amplitudes of the fundamental and second harmonic frequencies as a function of the phase R.

A key to reconstructing the amplitudes of the fundamental and second harmonic frequencies is to utilize both the magnitude and phase information provided by the signal's frequency spectrum. This information shown in Figs. 8 and 9 may be used to determine the amplitudes of Eqns. (8) and (9). Fig. 10 shows the amplitudes of the fundamental and second harmonics reconstructed from the data of Figs. 8 and 9. Notice that the amplitude of the fundamental harmonic varies sinusoidally as a function of R and the second harmonic varies cosinusoidally as a function of R. This data applied to Eqn. (10) may be used with an inverse tangent approximation to determine the desired phase R over a full 2π phase interval. This forms the kernel of the frequency domain demodulation algorithm. We have incorporated a fringe counting routine and verified the frequency domain demodulation algorithm through computer simulation.

In this section, we have verified the theoretical development of the previous section through computer simulation and described how to implement the algorithm in practice. A key step in the kernel of the frequency domain algorithm is use of both the magnitude and phase components of the frequency spectrum.

3.3 Discussion

We have presented a frequency domain approach to the demodulation of an interferometer, which uses a phased-generated carrier modulation scheme. Through simulation analysis, we have shown that the frequency domain algorithm produces correct demodulation results by assuming fixed operating parameters (i.e., $M=\pi$ and $W=0$). These are the same operating conditions as used in commercially-available time-domain demodulators.

Unfortunately, the frequency domain algorithm suffers from the same limitations as the time domain algorithm with regard to the carrier's modulation depth and phase. Drift of the carrier's modulation depth from $M = \pi$ produces a change in the amplitudes of the fundamental and second harmonic frequencies. This dependence manifests itself in the Bessel functions in Eqn. (7). If the value of this drift is unknown, it cannot be corrected in the computation of Eqn. (10) and errant demodulation results. Similarly, a drift of the carrier's modulation phase from $W = 0$ produces an irreparable change in the amplitudes of the harmonic frequencies.

As a consequence of these limitations, the frequency domain algorithm (like the time domain algorithm) requires careful initialization of the carrier's modulation depth and phase. Practical implementation of interferometric systems often use hardware, such as piezoelectric transducers, whose modulation depth drifts over time. Therefore, closed-loop active feedback is necessary to maintain the requisite modulation depth at $M = \pi$ rad.

3.4 Summary

We have presented the kernel of an algorithm for the digital demodulation of an interferometer based on the phase-generated carrier modulation scheme. This algorithm exploits both the magnitude and phase information in its frequency domain manipulation of the signal. The algorithm suffers from requirement that active feedback control is needed.

4. Conclusion

In this chapter, we have reviewed digital demodulation algorithms for interferometric metrology systems. Digital demodulation has the potential for producing a more robust and less costly sensor system. In general, the savings in optical and electronic hardware is traded-off with complex software algorithms. Consider the information shown in Table 1 of the specific digital demodulation techniques presented in this chapter.

Note that each of the digital demodulation methods presented in Table 1 is based on a homodyne approach. The heterodyne techniques require additional optical and electronic hardware to shift the frequency of one of the interfering optical beams. A key advantage of digital demodulation is a significant reduction in cost and hardware system complexity.

We have also presented a new demodulation algorithm for the well-known phase-generated carrier modulation scheme. Our algorithm is based on a frequency domain approach and requires both the magnitude and phase information present in the signal. This demodulation scheme suffers from the need for active feedback control. One possible approach to ameliorate this limitation is to investigate the use of a more sophisticated modulation signal. In the demodulation algorithm presented in Section 3, the carrier signal is a pure sinusoid and the desired output is the fixed phase R. We have studied interferometers, which use the phase-generated carrier modulation scheme and detect the amplitude of a *sinusoidally* varying phase $R(t)$. These systems produce harmonics, which we detect and then compute their ratio to remove the dependence on unknown quantities.

Demodulation Technique	Phase-generated carrier (time domain)	Phase-generated carrier (frequency domain)	J1 ... J4	3x3 fiber coupler
Application	Biological cell contraction measurement	Down-hole oil well drilling bit parameter measurement	MEMS vibrating amplitude measurement	Ballistic shock (velocity) measurement
Homodyne/Heterodyne	Homodyne	Homodyne	Homodyne	Homodyne
Passive/Active	Active	Active	Passive	Passive
Real-time/Post-processing	Real-time processing	Real-time processing	Real-time processing	Post-processing

Table 1. Comparison of digital demodulation techniques presented in this chapter.

It may be possible to design a carrier signal, which produces an appropriate set of harmonics that can be mathematically manipulated to cancel out any variations in M and W, yet still be solvable for the fixed phase R. The trade-off would be a true open-loop system, which would not require stringent initialization procedures, at the expense of a sophisticated carrier modulation signal. Further investigation into the viability of this approach is suggested.

5. Acknowledgment

The authors would like to recognize funding support from Weatherford International, Inc. for research related to the phase-generated carrier demodulation scheme presented in Sec. 3.

6. References

Barbour, N. & Schmidt, G., Inertial sensor technology trends. *IEEE Sensors Journal*, vol. 1, no. 4, (December 2001), pp. 332-339

Bush, J., Davis, C. A., McNair, F., Cekorich, A., & Bostick, J., Low cost fiber optic interferometric sensors.*Proceed. of the SPIE – Second Pacific Northwest Fiber Optic Sensor Workshop*, vol. 2872, (May 1996), pp. 1-12.

Cekorich, A., Bush, J., & Kirkendall, C., Multi-channel interferometric demodulator. *Proceed. of the SPIE – Third Pacific Northwest Fiber Optic Sensor Workshop*, vol. 3180, (May 1997), pp. 1-11.

Cekorich, A., Demodulator for interferometric sensors.*Proceed. of the SPIE*, vol. 3860, (December 1999), pp. 338-347.

Cole, J. H., Danver, B. A., & Bucaro, J. A., Synthetic-heterodyne interferometric demodulation. *IEEE J. Quantum Electron.*, vol. QE-18, no. 4, (April 1982), pp. 694-697.

Culshaw, B. & Giles, I. P., Frequency modulated heterdyne optical fiber Sagnac interferometer. *IEEE J. Quantum Electron.*, vol. QE-18, no. 4, (April 1982), pp. 690-693).

Dandridge, A., Tveten, A. B., & Giallorenzi, T. G., Homodyne demodulation scheme for fiber optic sensors using phase generated carrier.*IEEE J. Quantum Electron.*, vol. QE-18, no. 10, (October 1982), pp. 1647-1653.

Davis, P. G., Bush, I. J., & Maurer, G. S., Fiber optic displacement sensor.*Proceed. of the SPIE – Fourth Pacific Northwest Fiber Optic Sensor Workshop*, vol. 3489, (September 1998), pp. 18-22.

Fabiny, L. & Kersey, A. D., Interferometric fiber-optic Doppler velocimeter with high-dynamic range. *IEEE Photonics Technol. Lett.*, vol. 9, no. 1, (January 2997), pp. 79-81.

Jackson, D. A., Priest, R., Dandridge, A., & Tveten, A. B., Elimination of drift in a single-mode optical fiber interferometer using a piezoelectrically stretched coiled fiber. *Appl. Opt.*, vol. 19, no. 17, (September 1980), pp. 2926-2929.

Jackson, D. A., Kersey, A. D., Corke, M., & Jones, J. D. C., Pseudoheterodyne detection scheme for optical interferometers. *Electron. Lett.*, vol. 18, no. 25, (December 1982), pp. 1081-1083.

Jin, W., Zhang, L. M., Uttamchandani, D., & Culshaw, B., Modified J1...J4 method for linear readout of dynamic phase changes in a fiber-optic homodyne interferometer. *Appl. Opt.*, vol. 30, no. 31, (November 1991), pp. 4496-4499.

Jin, W., Walsh, D., Uttamchandani, D., & Culshaw, B., (1992). A digital technique for passive demodulation in a fiber optic homodyne interferometer. *1st European Conf. On Smart Structures and Materials*, Glasgow, UK, pp. 57-60.

Johnson, G. A., Todd, M. D., Althouse, B. L., & Chang, C. C., Fiber Bragg grating interrogation and multiplexing with a 3x3 coupler and a scanning filter. *J. Lightwave Technol.*, vol. 18, no. 8, (August 2000), pp. 1101-1105.

Kaplan, A. & Ruschin, S., Layout for polarization insensitive modulation in $LiNbO_3$ waveguides. *IEEE J. Selected Topics in Quantum Electron.*,vol. 6, no. 1., (January 2000), pp. 83-97.

Kern, J., Dimitrijevich, S. D., Tayag, T. J., Pitt, B. D., Summers, T. H., & Davis, C. G., An optical system to characterize the gross contractile response of a tissue-equivalent collagen matrix. *Proceed. of the SPIE - Optical Technologies to Solve Problems in Tissue Engineering,* vol. 4961, (January 2003), pp. 244-249.

Koo, K. P., Tveten, A. B., & Dandridge, A., Passive stabilization scheme for fiber interferometers using (3x3) fiber directional couplers. *Appl. Phys. Lett.*, vol. 41, no. 7, (October 1982), pp. 616-618.

Kumar, P., Thomas, A., Weis, R. S., & Tayag, T. J., Digital processing of an interferometric velocimeter for ballistic shock measurement. *Proceed. of the SPIE – Optical Inspection and Metrology for Non-Optics Industries*, vol. 7432, (2009).

Kwon, I. B., Kim, C. G., & Hong, C. S., A digital signal processing algorithm for structural strain measurement by a 3x3 passive demodulated fiber optic interferometer sensor. *Smart Materials & Structures*, vol. 8, (1999), pp. 433-440.

Marcal, L. A. P., Leao, J. V. F., Nader, G., Higuti, R. T., Kitano, C., & Silva, E. C. N., Analysis of linearity and frequency response of a novel piezoelectric flextensional actuator using a homodyne interferometer and the J1-J4 method. *IEEE Trans. on Instrumentation and Measurement*, vol. 56, no. 3, (June 2007), pp. 954-961.

Osten, W., Garbusi, E., Fleischle, D., Lyda, W., Pruss, C., Reichle, R., & Falldorf, C., Optical metrology – from the laboratory to the real world. *Proceed. of the SPIE – Speckle 2010: Optical Metrology*, vol. 7387, (2010).

Pitt, B. D., Tayag, T. J., & Nelson, M. L., Digital demodulation of an interferometer for the characterization of vibrating microstructures.*Proceed. of the SPIE – Advance Semiconductor Characterization Tech. for Optics, Semiconductors, and Nanotechnologies*, vol. 5188, (August 2003), pp. 61-70.

Porte, H., Gorel, V., Kiryenko, S., Goedgebuer, J.-P., Daniau, W., & Blind, P., Imbalanced Mach-Zehnder interferometer integrated in micromachined silicon substrate for pressure sensor. *J. Lightwave Technol.*, vol. 17, no. 2, (February 1999), pp. 229-233.

Saida, T. & Hotate, K., General formula describing drift of inteferometer fiber-optic gyro due to Faraday effect: Reduction of the drift in twin-depo-I-FOG. *J. Lightwave Technol.*, vol. 17, no. 2, (February 1999), pp. 222-228.

Sheem, S. K., Optical fiber interferometers with [3x3] directional couplers: Analysis. *J. Appl. Phys.*, vol. 52, no. 6, (June 1981), pp. 3865-3872.

Sheem, S. K., Giallorenzi, T. G., & Koo, K., Optical techniques to solve the signal fading problem in fiber interferometers. *Appl. Opt.*, vol. 21, no. 4, (February 1982), pp. 689-693.

Sudarshanam, V. S. & Srivivasan, K., Linear readout of dynamic phase change in a fiber-optic homodyne interferometer. *Opt. Lett.*, vol. 14, no. 2, (January 1989), pp. 140-142.

Tayag, T. J., Quantum-noise-limited sensitivity of an interferometer using a phase generated carrier demodulation scheme. *Opt. Eng. Lett.*, vol. 41, no. 2, (February 2002), pp. 276-277.

Tayag, T. J., Kolesar, E. S., Pitt, B. D., Hoon, K. S., Marchetti, J., & Jafri, I. H., An optical fiber interferometer for measuring the *in situ* deflection characteristics of MEMS structures. *Opt. Engineer.*, vol. 42, no. 1, (January 2003), pp. 105-111.

Tayag, T. J. &Bachim, B., Simulation of an interferometric computed tomography system for intraocular lenses. *Proceed. of the SPIE – Interferometry XV: Applications*, vol. 7791, (2010).

Tayag, T. J., Htun, T., & Kolesar, E. S., Integration of a low-cost fiber interferometer with a MEMS probe station. *Proceed. of the SPIE – Interferometry XV: Applications*, vol. 7791, (2010).

Todd, M. D., Johnson, G. A., & Chang, C. C., Passive, light intensity-independent interferometric method for fibre Bragg grating interrogation. *Electron. Lett.*, vol. 35, no. 22, (October 1999), pp. 1970-1971.

Tselikov, A., de Arruda, J. U., & Blake J., Zero-crossing demodulator for open-loop Sagnac interferometers. *J. Lightwave Technol.*, vol. 16, no. 9, (September 1998), pp. 1613-1619.

Weber, R. A., Tayag, T. J., & Shannon, L. J., Digital demodulation algorithm for the interferometric characterization of RF MEMS structures. *Proceed.of the SPIE - Interferometry XII – Techniques and Analysis*, vol. 5531, (August 2004), pp. 315-322.

Modern Metrology Concerns

Edited by Dr. Luigi Cocco

ISBN 978-953-51-0584-8
Hard cover, 458 pages
Publisher InTech
Published online 16, May, 2012
Published in print edition May, 2012

"What are the recent developments in the field of Metrology?" International leading experts answer this question providing both state of the art presentation and a road map to the future of measurement science. The book is organized in six sections according to the areas of expertise, namely: Introduction; Length, Distance and Surface; Voltage, Current and Frequency; Optics; Time and Relativity; Biology and Medicine. Theoretical basis and applications are explained in accurate and comprehensive manner, providing a valuable reference to researchers and professionals.

How to reference

In order to correctly reference this scholarly work, feel free to copy and paste the following:

Tristan J. Tayag and R. Collins Watson (2012). Digital Demodulation of Interferometric Signals, Modern Metrology Concerns, Dr. Luigi Cocco (Ed.), ISBN: 978-953-51-0584-8, InTech, Available from: http://www.intechopen.com/books/modern-metrology-concerns/digital-demodulation-of-interferometric-signals

INTECH
open science | open minds

InTech Europe
University Campus STeP Ri
Slavka Krautzeka 83/A
51000 Rijeka, Croatia
Phone: +385 (51) 770 447
Fax: +385 (51) 686 166
www.intechopen.com

InTech China
Unit 405, Office Block, Hotel Equatorial Shanghai
No.65, Yan An Road (West), Shanghai, 200040, China
中国上海市延安西路65号上海国际贵都大饭店办公楼405单元
Phone: +86-21-62489820
Fax: +86-21-62489821

IntechOpen